RESEARCH PAPERS

Acta Cryst. (1998). D**54**, 16–24

Structure of a Monoclinic Crystal Form of Cytochrome *b*1 (Bacterioferritin) from *E. coli*

ALAIN DAUTANT,[a]* JEAN-BRICE MEYER,[a] JOSEPH YARIV,[a] GILLES PRÉCIGOUX,[a] ROBERT M. SWEET,[b] A. JOSEPH KALB (GILBOA)[c] AND FELIX FROLOW[c]

[a]*Unité de Biophysique Structurale, ERS133 CNRS, Université de Bordeaux 1, 33405 Talence, France,* [b]*Biology Department, Brookhaven National Laboratory, Upton, New York 11973-50000, USA, and* [c]*Faculty of Chemistry, The Weizmann Institute of Science, Rehovot, Israel. E-mail: precigou@maxime.cristal.u-bordeaux.fr*

(*Received 9 September 1996; accepted 6 May 1997*)

Abstract

Crystals of *E. coli* cytochrome *b*1, alias bacterioferritin, were grown from a low ionic strength solution. The resulting monoclinic $P2_1$ structure was solved by molecular replacement and refined using noncrystallographic symmetries applied to the fundamental unit, consisting of two protein subunits and a single haem. From the Patterson self-rotation results it was shown that the asymmetric unit of the monoclinic crystal consists of 12 such dimers and corresponds to a complete, nearly spherical, molecule of bacterioferritin (M_r = 450 kDa) of 432 point-group symmetry. It is thus the most symmetrical cytochrome. As previously determined for the tetragonal form, the haem is located in a special position on a local twofold axis of the dimer. A bimetal centre is also observed within the four-helix bundle of each monomer; a metal-binding site is located on the fourfold axis.

1. Introduction

Cytochrome *b*1 of *Escherichia coli* is bound to the bacterial membrane but can be solubilized by sonication. The soluble molecule was shown to have the quaternary structure of ferritin and, therefore, was called bacterioferritin (Yariv *et al.*, 1981). The structure of the tetragonal crystal form of bacterioferritin has been determined recently [Frolow, Kalb (Gilboa) & Yariv, 1994]. The structure determination shows that the metalloporphyrin site is unique in having, as haem axial ligands, the S atoms of two methionine residues related by a twofold symmetry axis.

E. coli bacterioferritin (EcBFR) is both a ferritin and a cytochrome (Yariv *et al.*, 1981; Bauminger *et al.*, 1980; St Pierre *et al.*, 1986). Its distinctive name was meant to underline the difference between bacterial and eukaryotic ferritin, the latter being classified as a 'non-haem iron protein' (Granick & Michaelis, 1943). Today this distinction is not as sharp as previously thought because of some new evidence. One piece of evidence is the discovery in *E. coli* of a protein that conforms to the definition of eukaryotic ferritin, that is to say a 'non-haem iron protein' (Izuhara, Takamune & Takata, 1991; Hudson *et al.*, 1993). Further evidence is that horse-spleen ferritin, the intensely studied eukaryotic ferritin (Granick & Michaelis, 1943), includes a cleft which can accommodate protoporphyrin IX in a site corresponding to the haem-binding site in bacterioferritin (Précigoux *et al.*, 1994). While the connection between iron storage by *E. coli* and the electron-transport activity of EcBFR remains open to question, there is no valid reason to suppose that the unique function of this cytochrome lies in the iron storage (*cf.* Andrews *et al.*, 1995). It should be pointed out that cytochromes with very similar spectral characteristics were observed by Keilin (1934) in other bacteria and in yeast. In this report we describe the structure and packing at 2.94 Å resolution of EcBFR in its low-salt monoclinic crystal form.

2. Results

2.1. *Crystallization, X-ray data collection and processing*

Prismatic monoclinic crystals were obtained by addition of traces of $MnCl_2$ to a protein solution extensively dialysed against distilled water, as described by Smith, Ford, Harrison, Yariv & Kalb (Gilboa) (1989). Film data were collected in 1986 at the National Synchrotron Light Source, BNL, on beamline X12c. The crystal was mounted with its twofold screw axis nearly parallel to the rotation axis. The wavelength was 1.22 Å and the crystal-to-film distance was set to 100 mm. The oscillation range was from 0.75 to 1.5° per film in order to minimize overlaps for different parts of the reciprocal lattice. A total data set over 90° was collected to a resolution of 2.8 Å. The crystal was wedge shaped; thus the time of exposure was adjusted to compensate roughly for path-length changes. Exposure times were adjusted automatically according to total beam flux and manually according to crystal thickness, such that there were approximately 2×10^6 counts per

degree rotation per mm thickness. A typical exposure time was approximately 30 min. Films, exposed in packs of three, interleaved with exposed film for attenuation, were developed immediately. They were scanned on a computerized Optronics drum scanner and the data were processed with the Purdue Data Processing Package (Rossmann, 1979; Rossmann, Leslie, Abdel-Meguid & Tsukihara, 1979) at the Purdue University Macromolecular Computing Center (supported by NSF facility grant 9102464-BIR to John E. Johnson). The space group is $P2_1$ (systematic absences $0k0$: $k = 2n$); the unit-cell has dimensions a = 118.7, b = 211.6, c = 123.3 Å, $\beta = 119.1°$, and contains two molecules. The data set is 84% complete between 46.7 and 2.94 Å (94 076 unique reflections; $R_{sym} = 0.12$ on intensities). A summary of crystal, data collection and refinement data is given in Table 1.

Table 1. *Crystal, data collection and refinement data*

Space group	$P2_1$
Cell dimensions (Å, °)	
a	118.7
b	211.6
c	123.3
β	119.1
Bacterioferritin molecules per unit-cell	2
Asymmetric unit	24 proteins, 12 haem molecules, 54 Mn ions
X-ray source	National Synchrotron Light Source (λ = 1.22 Å)
Resolution (Å)	46.7–2.94
Independent measurements	94076
R_{sym}	0.12
Completeness (%)	
10–2.94 Å resolution	84
3.02–2.99 Å	72
2.99–2.96 Å	72.9
2.96–2.94 Å	42.7
R	0.22
R.m.s. deviations (Å, °)	
Bond lengths	0.01
Bond angles	2.3

2.2. *Structure solution of the monoclinic crystal*

For standard and locked self-rotation, the general and locked rotation function (*GLRF*) program was used (Tong & Rossmann, 1990).

The results of the self-rotation function reported here were computed with the 5499 structure-factor amplitudes greater than two times the average of all structure factors, from the 57 838 reflections between 8 and 3 Å resolution. The Patterson origin was removed and the radius of integration set to 80 Å. The search was performed with intervals of 2° with κ set at 180, 120 and 90° (Figs. 1*a*, 1*b* and 1*c*) in order to establish the orientation of the noncrystallographic two-, three- and fourfold axes, respectively. The rotation function was contoured at intervals of 1σ, starting from 1σ. All projections correspond to the superimposition of two stereographic projections of a 432 point-group symmetry related by the *ac* mirror plane. Thus, the results lead to a standard tetraeicosahedron (fourfold axes initially coincident with the reference frame axes) rotated by $\kappa = 24°$ about an axis given by $\varphi = 136°$ and $\psi = 96°$.

This orientation was confirmed by a locked self-rotation function using the same data subset in which the 432 point-group symmetry was included. Three-dimensional searches around $\kappa = 24°$ produced a maximum peak (5σ above the background) centred at $\kappa = 24.1°$, $\varphi = 135.8°$ and $\psi = 96.5°$ (Fig. 1*d*).

The structure was solved by molecular replacement. The starting model was generated from the coordinates of the recently solved structure of the $P4_22_12$ crystal form of EcBFR, with unit-cell dimensions $a = b = 211.1$, c = 145.2 Å (Brookhaven Protein Data Bank; entry code 1BCF). From these coordinates we built a 24-mer by applying each of the noncrystallographic symmetry operations, as defined in the 1BCF header, and the twofold crystallographic axis of $P4_22_12$. The model included the backbone and Cβ atoms of a complete tetraeicosahedron (the asymmetric unit in $P2_1$). In order to facilitate comparison of the results of the Patterson cross- and self-rotation searches, the fourfold axes of the model were initially set to coincide with the orthogonal reference frame axes. Cross-rotation, translation functions and rigid-body refinement were performed with the *AMoRe* program package (Navaza, 1992).

All diffraction data in the resolution range 10–5 Å were included in the rotation function using a cut-off radius of 30 Å. The rotation function displayed 24 equivalent solutions (peak height > 5σ), which are related to one another by the noncrystallographic symmetries (NCS) obtained from the self-rotation function. The best solution of the translation function corresponding to a 5σ peak height (correlation coefficient = 0.37, R factor = 0.48) predicted the centre of the molecule to be at ($x_c = 0.427$, y_c, $z_c = 0.201$). After rigid-body refinement, the correlation coefficient was 0.655 and the R factor was 0.42. The refined orientation of EcBFR is related to the standard dodecahedron orientation by a rotation $\kappa = 24.3°$, $\varphi = 136.2°$ and $\psi = 97.3°$, in excellent agreement with the self-rotation results.

2.3. *Refinement*

Standard and locked self rotations showed that proper NCS, corresponding to an ideal 432 point group with all intersecting n-fold axes and without screw components, were an adequate representation of the structure at 2.9 Å resolution. In order to have simple forms for the NCS relations, a skew frame was defined with its axes coincident with the fourfold axes of the molecule.

The molecule, without haem moieties, was first refined as a rigid body with the 24-mer as a single group. At this stage, a difference Fourier map clearly showed well

defined residual density corresponding to the haem molecule with its quasi-dyad axis closely aligned with the pseudo-dyad of each dimer. Consequently, the structure was refined with a model constituted of one dimer and its associated haem molecule and assuming that the 12 NCS-related subunits were strictly identical. All side chains (Andrews, Smith, Guest & Harrison, 1989) were added to the model by inspection of $F_o - F_c$ and $2F_o - F_c$ electron-density maps. The refinement calculations were interleaved with several inspections

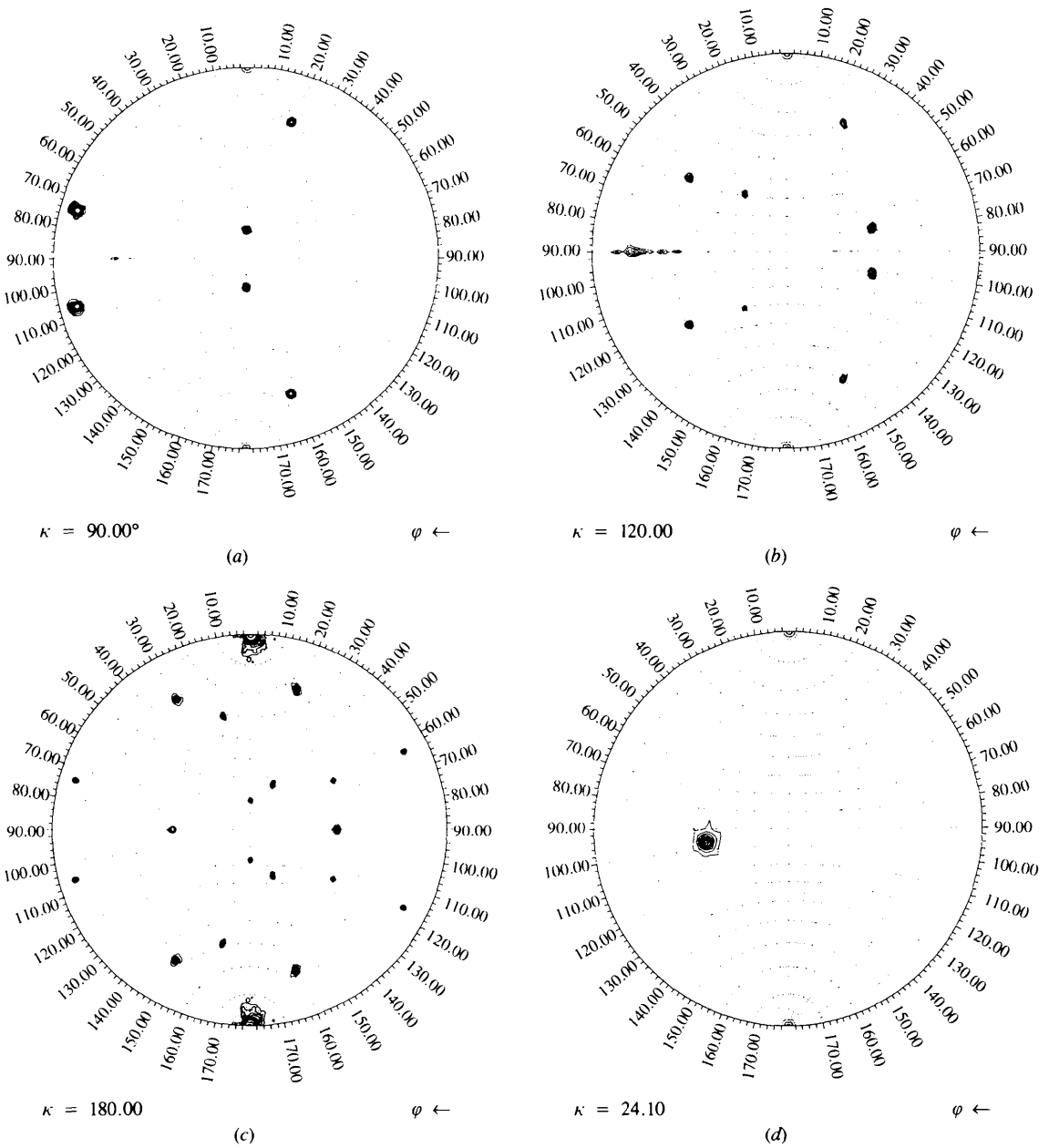

Fig. 1. The orthogonalization convention employed aligns the real-space a axis along the Cartesian axis x, and $a \times b$ (c^*) coincides with the z axis. The polar coordinates ψ, φ and κ are defined by Rossmann & Blow (1962). (*a*) Stereographic projection at $\kappa = 90°$ showing the fourfold peaks ($\psi = 24$, $\varphi = 45$; $\psi = 73$, $\varphi = 90$; $\psi = 74$, $\varphi = 175°$). (*b*) Stereographic projection at $\kappa = 120°$ showing the threefold peaks ($\psi = 30$, $\varphi = 40$; $\psi = 58$, $\varphi = 148$; $\psi = 59$, $\varphi = 116$; $\psi = 78$, $\varphi = 43°$). (*c*) Stereographic projection at $\kappa = 180°$ showing the twofold peaks ($\psi = 33$, $\varphi = 151°$; $\psi = 63$, $\varphi = 9°$; $\psi = 64$, $\varphi = 77°$; $\psi = 66$, $\varphi = 42°$; $\psi = 31$, $\varphi = 113°$; $\psi = 90$, $\varphi = 132°$) and the fourfold peaks. Note the special position of one twofold axis of the 432 point group ($\psi = 90$, $\varphi = 132°$) perpendicular to the twofold axis of the $P2/m$ space group that generates one extra twofold NCS at $\psi = 90°$, $\varphi = 42°$. (*d*) Locked self-rotation function results. A single peak at $\kappa = 24.1°$ is found for $\psi = 96.5°$ and $\varphi = 135.8°$.

and manual adjustments of the lateral chain positions with the program *TURBO-FRODO* (Roussel, Fontecilla-Camps & Cambillau, 1990). Positional refinement and restrained individual isotropic *B*-factor refinement were carried out with *X-PLOR* (Brünger, 1990).

The final refinement led to a crystallographic *R* factor of 0.22 for 91 554 reflections between 10 and 2.94 Å resolution and with amplitudes greater than 2σ. The final skew rotation and skew vector are (κ = 335.96, φ = 135.94, ψ = 96.50°) and (38.545, −6.142, 21.716 Å), respectively. The r.m.s. deviations from ideality for bond lengths, bond angles, dihedral angles and improper angles are 0.01 Å, 2.3, 19 and 1.7°, respectively. The average *B* factor for all protein atoms is 11 Å^2.

A Ramachandran plot (Ramachandran & Sasisekharan, 1968) is shown in Fig. 2. All the residues are in the allowed regions, with 97% being within the most energetically favourable regions.

Atomic coordinates and structure factors have been deposited with the Protein Data Bank, Brookhaven National Laboratory.†

Attempts to refine independently the 12 NCS led to the following orientations of the cubic symmetry axes: fourfold axes 90.01 (10)°; twofold axes 179.97 (7)°; threefold axes 119.98 (7)°. The amplitude of the screw vectors was only 0.21 (8) Å and introduction of improper rotations did not bring about a significant decrease in the crystallographic *R* factor.

† Atomic coordinates and structure factors have been deposited with the Protein Data Bank, Brookhaven National Laboratory (Reference 1BFR, R1BFRSF). Free copies may be obtained through the Managing Editor, International Union of Crystallography, 5 Abbey Square, Chester CH1 2HU, England (Reference GR0673).

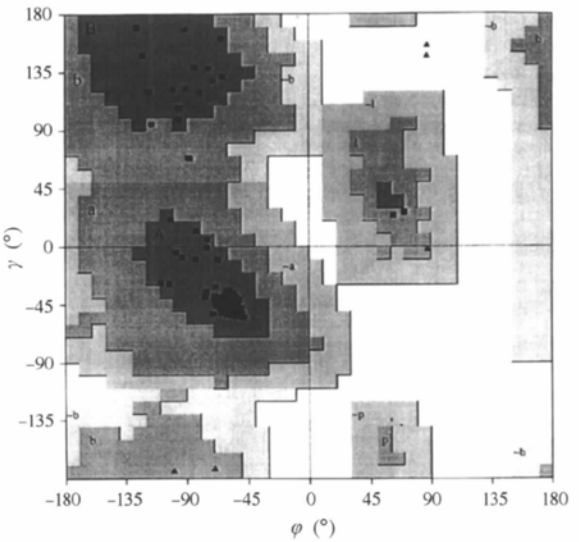

Fig. 2. Ramachandran plot for main-chain torsion angles (φ, ψ). The shading parts indicate allowed regions of conformational space (Laskowski, MacArthur, Moss & Thornton, 1993). Triangles denote glycine residues, squares all others. The figure was produced using the program *PROCHECK* (Morris, MacArthur, Hutchinson & Thornton, 1992).

2.4. *Description of the molecule*

The EcBFR monomer is made of four long *A*, *B*, *C* and *D* helices which form the usual square left-handed bundle (Harris, Presnell & Cohen, 1994) observed for ferritin molecules. The four-helix bundle is composed of two antiparallel helix pairs, *AB* and *CD*, extending from Thr5 to Trp35 and from Lys38 to Phe64 for *AB*, and from Val83 to Val111 and Tyr114 to Met144 for *CD* (Fig. 3). A fifth short *E* helix, Leu146–Gln151, at the C-terminal, lies almost perpendicular (78°) to the bundle axis.

From Leu65 to Asp82, an overhang connection of 18 residues (*L* loop), spans the length of the bundle connecting the *B* and *C* helices.

The carboxylic ends of helices *A*, *B* and *C* contain hydrogen bonds of type 1–4 and can be considered as type I β-turns. Each of these β-turns, with Asn34–Trp35 (*AB* turn), Phe64–Leu65 (*BL* turn) and Ser110–Val111 (*CD* turn) as corner residues, are enhanced by one extra 1–6 hydrogen bond. Whereas turn *AB* is only present in EcBFR, turns *BL* and *CD* are also observed in horse-spleen ferritin (1HRS) and human H-chain ferritin (1FHA). A tight turn, involving residues Met144 and Gly145, is observed at the junction between *D* and *E* helices. Such a turn is also observed in the crystal structure of amphibian red-cell L ferritin (Trikha, Theil & Allewell, 1995). The connection between the *L* loop and helix *C* adopts a random coil conformation.

In contrast with the eukaryotic ferritins, the fourfold channels are extremely hydrophilic with four Asn148 residues on the outer surface of the protein shell and four Gln151 residues bound to a heavy atom, on the inner surface (Fig. 4). Considering the peak height and the fact that $MnCl_2$ was included in the medium, we introduced an Mn atom at this position during the refinement process. The final *B* factor for the presumed Mn ion is 12 Å^2. The threefold channels, similarly hydrophilic, are lined with Asp109, Arg117 and Asp118. The assembly of 24 subunits forms a slightly distorted spherical shell with inner and outer diameters of 75 and 120 Å, respectively.

As described for the tetragonal form of bacterioferritin [Frolow, Kalb (Gilboa) & Yariv, 1994], all four helices, *A*, *B*, *C* and *D*, participate in the ligation of two non-haem metal atoms through six residues, namely Glu18; Glu51 and His54; Glu94; and Glu127 and His130. These six ligands are highly conserved in bacterioferritin sequences (Fig. 3). Until now, the only mutation in the bimetal centre was observed for *Mycobacter avium* (Inglis, Stevenson, Hosie & Sharp, 1994) where Glu18 is replaced by Gln. At the present resolution, no solvent molecule is observed as a metal ligand. The two metal ions are separated by a distance of 4.36 Å and a close examination of the $F_o - F_c$ maps does not reveal any

electron density between them. Earlier EPR and MCD spectroscopic studies revealed the presence of two mononuclear reduced non-haem iron sites (Cheesman *et al.*, 1993). Whether these sites correspond to the bimetal centre described by us remains to be established.

Among the charged interactions, we note that Glu128, the nearest neighbour of the Glu127 metal ligand, forms an inter-subunit salt bridge with the threefold-axis-related Arg61 residue (2.75 and 2.95 Å). Glu128 also participates in an intra-subunit salt bridge with Arg102 (2.70 Å), linking the *C* and *D* helices. While the Glu residues are conserved, Arg102 can be replaced by Lys.

On the outer surface of the molecule, the stability of the dimer is enhanced by four hydrogen bonds (Fig. 5) between the O and N atoms of the amide function of the conserved Gln72 residue and N (Leu77) and O (Gly75) atoms of a neighbouring subunit main chain. On the inner surface, a salt bridge is observed between Arg30 (*A* helix) and Asp56, Glu60 (*B* helix). While residue 60 is not at all conserved, residues 30 and 56 can only be replaced by other basic or acidic residues, respectively.

Despite the lack of sequence homology between EcBFR and eukaryotic ferritins (18% identity between EcBFR and horse-spleen ferritin), their secondary structures are very similar (Fig. 6). The r.m.s. deviation between 141 equivalent Cα positions of EcBFR and horse-spleen ferritin is 1.8 Å. Significant differences in Cα positions are only observed in the loops and turns connecting helices and in the C-termini of the proteins.

2.5. *The haem binding site*

The haem binding site in the low ionic strength structure is identical to that observed in the high ionic

```
1           11          21          31          41          50
MKGDTKVINY LNKLLGNELV AINQYFLHAR MFKNWGLKRL NDVEYHESID          E. coli
MKGDKIVIQH LNKILGNELI AINQYFLHAR MYEDWGLEKL GKHEYHESID          A. vinelandii
MQGDPDVLRL LNEQLTSELT AINQYFLHSK MQENWGFTEL AERTRVESFD          M. leprae
MQGDPEVLRL LNEQLTTQLT AINQYFLHSK MQDNWGFTEL AEHTRAESFD          M. avium
MKGDAKVIEF LNAALRSELT AISQYWVHFR LQEDWGLAKM AKKSREESIE          R. capsulatus
MKGEPKVIER LNDALFLELG AVNQYWLHYR LLNDWGYTRL AKKEREESIE          B. melitensis
MQGHPEVIDY LNTLLTGELA ARDQYFIHSR MYEDWGFSKL YERLNHEMEE          P. aerugisona a
MKGDKKVIQH LNKILGNELI AINQYFLHSR MWNDWGLKRL YAHLYHESID          P. aerugisona b
MKGKPAVLAQ LHKLLRGELA ARDQYFIHSR MYQDWGLEKL YSRIDHEMQD          C. Synechocystis
MKGDPKVIDY LNKALRHELT AINQYWLHYR LLDNWGIKDL AKKWRAESIE          N. winogradskyi
MQGDPEVLRL LNEQLTSELT AINQYFLHSK MQDNWGFTEL AE                   M. paratuberculosis

51          61          71          81          91          100
EMKHADRYIE RILFLEGLPN LQDLGKLNIG EDVEEMLRSD LALELDGAKN          E. coli
EMKHADKLIK RILFLEGLPN LQELGKLLIG EHTKEMLECD LKLEQAGLPD          A. vinelandii
EMRHAEAITD RILLLDGLPN YQRIGSLRVG QTLREQFEAD LAIEYEVMSR          M. leprae
EMRHAEAITD RILLLDGLPN YQRLFSLRIG QTLREQFEAD LAIEYEVMDR          M. avium
EMGHADKIIA RILFLEGHPN LQKLDPLRIG EGPRETLECD LAGEHDALKL          R. capsulatus
EMHHADKLIN RIIFFEGFPN LQTVSPLRIG QNVKEVLEAD LKGEYDARAS          B. melitensis
ETQHAXXLLR RILXLEGTP                                            P. aerugisona a
EMKXA                                                           P. aerugisona b
ET HA                                                           C. Synechocystis

101         111         121         131         141         150
LREAIGYADS VHDYVSRDMM IEILRDEEGH IDWLETELDL IQKMGLQNYL          E. coli
LKAAIAYCES VGDYASRELL EDILESEEDH IDWLETQLDL IDKIGLENYL          A. vinelandii
LKPGIIMCRE KQDSTSAVLL EKIVADEEEH IDYLETQLAL MGQLGEELYS          M. leprae
LKPAIILCRE KQDSTTATLF EQIVADEEKH IDYLETQLEL MDKLGVELYS          M. avium
YREARDYCAE VGDIVSKNIF ESLITDEEGH VDFLETQISL YDRLGPQGFA          R. capsulatus
YKESREICDK LGDYVSKQLF DELLADEEGH IDFLETQLDL LAKIGEERYG          B. melitensis

151
QAQIREEG                                                        E. coli
QSQMDE                                                          A. vinelandii
AQCVSRPPS                                                       M. leprae
AQCVSRPPS                                                       M. avium
LLNAAPMDAA E                                                    R. capsulatus
QLNAAPADEA E                                                    B. melitensis
```

Fig. 3. Sequence alignment of bacterioferritins.

strength tetragonal form of EcBFR [Frolow, Kalb (Gilboa) & Yariv, 1993], the axial iron ligands being two Met52 residues related by a noncrystallographic twofold axis. Met52 is a well conserved residue in the bacterioferritin family although an alteration Met52→Thr52 is reported for *Pseudomonas aeruginosa* (*a*) (Moore *et al.*, 1994) and *Cyanobacterium synechocystis* (Laulhère, Laboure, van Wuytswinkel & Gagnon, 1992) (Fig. 3). These two sequences are, however, preliminary results. The haem binding site is located on the inner side of the protein and is close to two symmetry-related bimetal centres (Fig. 7); the distances between the haem Fe atom and the two non-haem metal atoms are 14.5 and 12.8 Å. The hydrophobic pocket, which encloses the haem, forms an indentation opening from the surface of the inner cavity and creeping along the hydrophobic interface between two subunits. The pocket is lined with residues Leu19, Ile22, Asn23 and Phe26 (*A* helix), Tyr45, Ile49, Met52, Lys53, Ala55 and Asp56 (*B* helix), Leu71 of the *L* loop, and the equivalent twofold-axis-related residues. The haem molecule is only accessible from the inside of the protein shell, where its two propionate groups protrude into the hydrophilic internal cavity, and is protected against the outside aqueous medium by the two symmetry-related *L* loops.

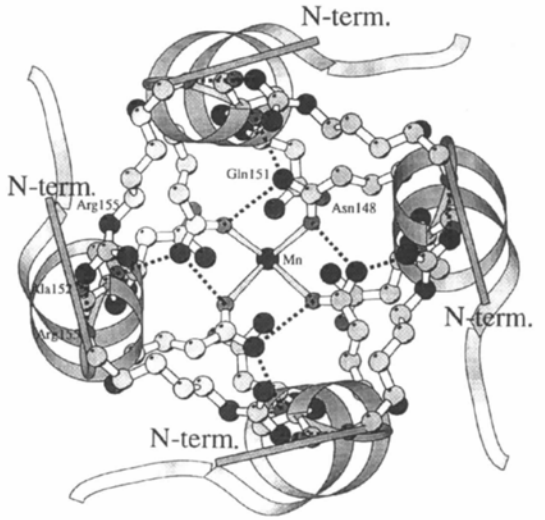

Fig. 4. View along the fourfold channel. A residual density is attributed to a Mn atom linked to four symmetrically related Gln151 residues. The ribbon drawings were generated with *MOLSCRIPT* (Kraulis, 1991) and rendered with *RASTER3D* (Bacon & Anderson, 1988).

2.6. *Crystal packing*

Except for the atoms interacting through the $P2_1$ symmetry operator, atomic level interactions cannot be specified because of the assumption that all NCS-related subunits are strictly identical.

If we consider the bacterioferritin molecules as hard spheres, the crystal packing can be described as quasi-hexagonal layers ($a \simeq c$; $\beta \simeq 120°$) stacked along the b axis. Assuming a mean molecular radius of about 61 Å,

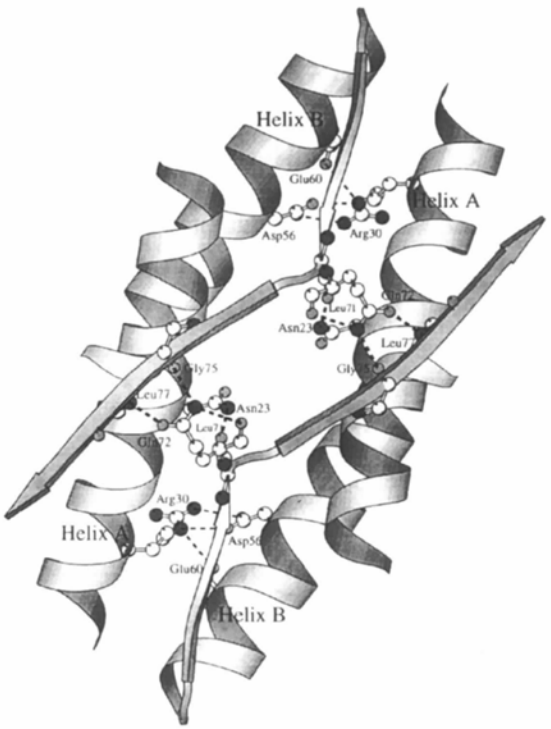

Fig. 5. View along the twofold axis of a dimer showing hydrogen bonds between the subunits.

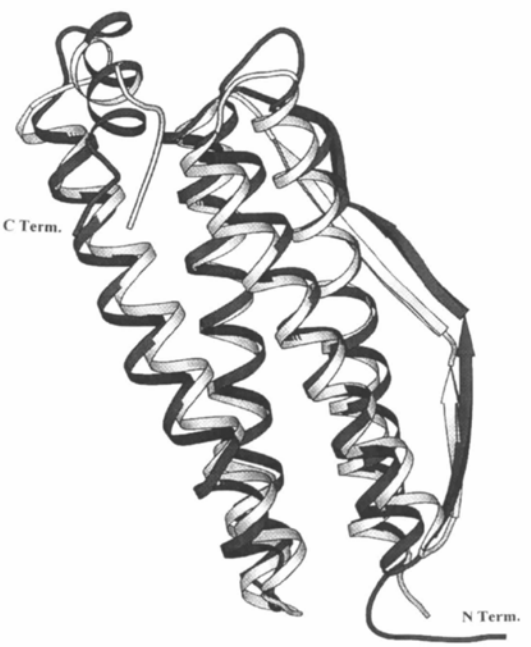

Fig. 6. View showing the superimposition of the EcBFR (light grey) and horse-spleen ferritin (dark grey) Cα traces.

the resulting hard-sphere unit-cell occupancy of 0.7 is close to an orthorhombic all-face-centred unit-cell occupancy.

In the *ac* plane, each molecule is surrounded by six neighbours related by pure lattice translations, with distances between the molecular centres of $a = 118.7$, $b = 123.3$ and $|a + c| = 122.7$ Å. There are three types of intralayer intermolecular contacts between a given molecule and its neighbours, as described below.

(i) Since one of the noncrystallographic fourfold axes ($\psi = 107$ or $73°$, $\varphi = 90°$) is perpendicular to a lattice crystallographic *a* axis, an additional noncrystallographic twofold axis occurs parallel to the fourfold axis through $(\frac{1}{2} + x_c, y_c, z_c)$. Crystal contacts along [100] are between the C-terminal residues of the *CD* turns of two molecules related by the additional twofold axis. Moreover, the C-terminal residues of the *CD* turns interact with the *DE* turns.

(ii) Similarly, the noncrystallographic twofold axes ($\psi = 33$ or $147°$, $\varphi = 151°$) perpendicular to *c* yield additional noncrystallographic twofold axes through $(x_c, y_c, \frac{1}{2} + z_c)$ parallel to the twofold axes. Crystal contacts along [001] are between the N-terminal coils of two molecules related by this local twofold axis. The N-terminal coils of one molecule interact with the end of the *B* helix of the second molecule.

(iii) Along [101] around $(\frac{1}{2} + x_c, y_c, \frac{1}{2} + z_c)$ the *L* loop interacts with the *C* helix.

The adjacent layers are related by the twofold screw axis. Along the *b* axis, each molecule is surrounded by four symmetry-related molecules with distances between their molecular centres of 121.6 and 125.2 Å. Two other molecules are too far away (138 Å) and do not participate in any intermolecular interactions. Interlayer contacts occur as follows: (i) around $(\frac{1}{2}, \frac{1}{4} + y_c, 0)$ between the threefold and fourfold channels, where the molecules are packed *via* contacts between their threefold vertices; (ii) at $(\frac{1}{2}, \frac{1}{4} + y_c, \frac{1}{2})$ between the N-terminal coil and the end of the long interhelical loop.

In agreement with the relatively long distance (125.2 Å) observed between the centres of two adjacent molecules, only a few interactions are observed.

3. Discussion

The monoclinic structure of *E. coli* cytochrome *b*1 has been solved by molecular replacement and refined to 2.94 Å resolution. Despite this relatively low resolution, some interesting features have emerged from this structure. From the Patterson self-rotation results it was shown that the asymmetric unit of the monoclinic crystal consists of 12 dimers and corresponds to a complete, nearly spherical, molecule. Furthermore, we confirmed that the haem is located on a twofold axis, at the interface between two subunits with the S atoms of the symmetry-related Met52 residues as axial iron ligands.

In the bimetal centre, the metal atoms are bridged by the carboxylate groups of Glu51 and Glu127. The geometries of the pseudo-octahedral metal coordination states are distorted in the plane of their bidentate ligands Glu18 and Glu94. The two histidine ligands bind to the metal atoms through their N^{δ} atoms (Fig. 8).

The same binding mode is observed for the bimetallic centres of ribonucleotide reductase (Nordlund & Eklund, 1993), methane mono-oxygenase (Rosenzweig, Frederick, Lippard & Nordlund, 1993) and the H chain of human ferritin (Lawson *et al.*, 1991) where the N^{ε} atoms of the corresponding histidine residues, His54 and

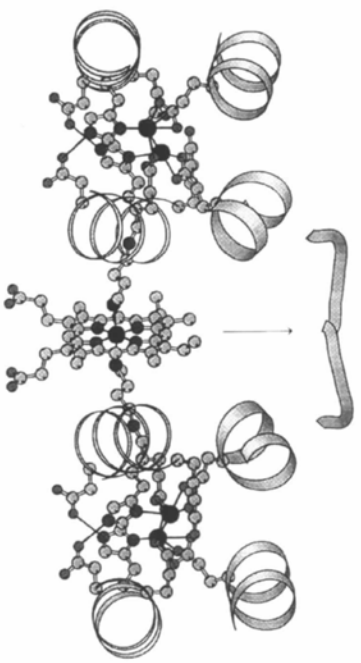

Fig. 7. View showing the haem location relative to the symmetry-related bimetal centres.

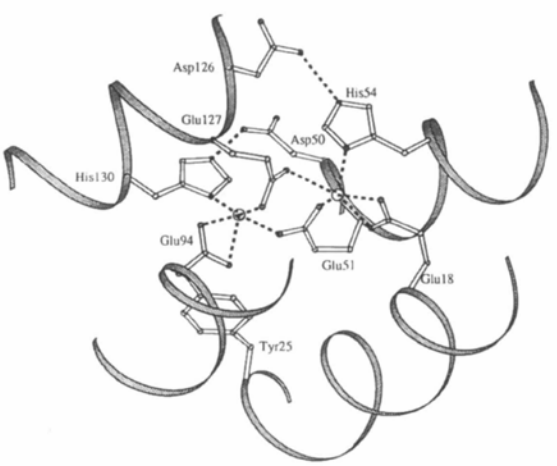

Fig. 8. The bimetal centre.

His130, bind to the carboxyl O atoms of Asp126 and Asp50, respectively.

Asp50 and Asp126 are often conserved in bacterioferritin sequences but can be replaced by Glu in *P. aeruginosa* (*a*) (Moore *et al.*, 1994), *Nitrobacter winogradskyi* (Kurokawa, Fukumori & Yamanaka, 1989), *Rhodobacter capsulatus* (Penfold, Ringeling, Moore, McEwan & Spiro, 1996) and *Brucella melitensis* (Denoel *et al.*, 1995), or by Ser in *Azotobacter vinelandii* (Grossman, Hinton, Minak-Bernero, Slaughter & Stiefel, 1992).

The same situation is observed in two other binuclear metal proteins, myohemerythrin (Sheriff & Hendrickson, 1987) and hemocyanin (Magnus, Lattman, Volbeda & Hol, 1991) where the metal atoms are coordinated to the N^{ε} atoms of histidine residues.

A tyrosine, which corresponds to Tyr58 in EcBFR, is observed in the active site of ribonucleotide reductase. The distances between the hydroxyl group of Tyr58 and the nearest metal atom are 5.9 and 5.3 Å in EcBFR and ribonucleotide reductase, respectively. Nevertheless, this amino acid is present only in EcBFR and is replaced by a hydrophobic residue (Ile or Leu) in the other bacterioferritins (Fig. 3). However, another tyrosine, Tyr25, is always conserved in BFRs and also in eukaryotic ferritins. The hydroxyl O atom of Tyr25 points towards the metal centre with a distance of only 3.6 Å from the closest metal ion.

The monoclinic crystal form of cytochrome *b*1 was grown from a very dilute salt solution and it is significant that the molecule that crystallized is the same as the one in the tetragonal crystal, which grew in 50% saturated ammonium sulfate. This is especially significant since it has been recently demonstrated that a solution of EcBFR contains, even if in a minute quantity, dimers as well as the 24-mer protein (Andrews, Smith, Hawkins, Williams & Harrison, 1993). It has to be recognized that the molecule of BFR that we report is very surprising and raises the question of how such a water-soluble molecule can be attached to the membrane of the cell and yet sediment with membranes on cell disruption (Keilin & Harpley, 1941; Deeb & Hager, 1964). It is only because nowadays we use sophisticated tools for breaking the bacteria that we obtain it in a soluble form (Yariv *et al.*, 1981). Since BFR can be obtained with the polynuclear iron compound filling the interior space, one cannot be confident that the assembly of the 24-mer molecule is not an artefact of the preparation. Therefore, the possibility that cytochrome *b*1 is associated with *E. coli* membrane in assemblies different from the one that we report here appears to be unlikely.

Diffraction data for this study were collected at Brookhaven National Laboratory in the Biology Department single-crystal diffraction facility at beamline X12-C in the National Synchrotron Light Source. This facility is supported by the United States Department of Energy, Office of Health and Environmental Research, and by the National Science Foundation.

References

Andrews, S. C., LeBrun, N. E., Barynin, V., Thomson, A. J., Moore, G. R. & Harrison, P. M. (1995). *J. Biol. Chem.* **270**, 23268–23274.

Andrews, S. C., Smith, J. M. A., Guest, J. R. & Harrison, P. M. (1989). *Biochem. Biophys. Res. Commun.* **158**, 489–496.

Andrews, S. C., Smith, J. M. A., Hawkins, C., Williams, J. M. & Harrison, P. M. (1993). *Eur. J. Biochem.* **213**, 329–338.

Bacon, D. J. & Anderson, W. F. (1988). *J. Mol. Graphics*, **6**, 219–220.

Bauminger, E. R., Cohen, S. G., Dickson, D. P. E., Levy, A., Ofer, S. & Yariv, J. (1980). *Biochim. Biophys. Acta*, **623**, 237–242.

Brünger, A. T. (1990). *X-PLOR Manual.* Version 2.1. Yale University, New Haven, USA.

Cheesman, M. R., Kadir, F. H., Thomson, A. J., Moore, G. R., Andrews, S. C., Guest, J. R., Harrison, P. M., Smith, J. M. & Yewdall, S. J. (1993). *Biochem. J.* **292**, 47–56.

Deeb, S. S. & Hager, L. P. (1964). *J. Biol. Chem.* **239**, 1024–1031.

Denoel, P. A., Zygmunt, M. S., Weynants, V. E., Tibor, A., Lichtfouse, B., Briffeuil, P., Limet, J. N. & Letesson, J. J. (1995). *FEBS Lett.* **361**, 238–242.

Frolow, F., Kalb (Gilboa), A. J. & Yariv, J. (1993). *Acta Cryst.* D**49**, 597–600.

Frolow, F., Kalb (Gilboa), A. J. & Yariv, J. (1994). *Nature Struct. Biol.* **1**, 453–460.

Granick, S. & Michaelis, L. (1943). *J. Biol. Chem.* **147**, 91–97.

Grossman, M. J., Hinton, S. M., Minak-Bernero, V., Slaughter, C. & Stiefel, E. I. (1992). *Proc. Natl Acad. Sci. USA*, **89**, 2419–2423.

Harris, N. L., Presnell, S. R. & Cohen, F. E. (1994). *J. Mol. Biol.* **236**, 1356–1368.

Hudson, A. J., Andrews, S. C., Hawkins, C., Williams, J. M., Izuhara, M., Meldrum, F. C., Mann, S., Harrison, P. & Guest, J. R. (1993). *Eur. J. Biochem.* **218**, 985–995.

Inglis, N. F., Stevenson, K., Hosie, A. H. F. & Sharp, J. M. (1994). *Gene*, **150**, 205–206.

Izuhara, M., Takamune, K. & Takata, R. (1991). *Mol. Gen. Genet.* **225**, 510–513.

Keilin, D. (1934). *Nature (London)*, **133**, 290–291.

Keilin, D. & Harpley, C. H. (1941). *Biochem. J.* **35**, 688- 692.

Kraulis, P. J. (1991). *J. Appl. Cryst.* **24**, 946–950.

Kurokawa, T., Fukumori, Y. & Yamanaka, T. (1989). *Biochim. Biophys. Acta*, **976**, 135–139.

Laskowski, R. A., MacArthur, M. W., Moss, D. S. & Thornton, J. M. (1993). *J. Appl. Cryst.* **26**, 283–291.

Laulhère, J. P., Laboure, A. M., van Wuytswinkel, O. & Gagnon, J. (1992). *Biochem. J.* **281**, 785–793.

Lawson, D. M., Artymiuk, P. J., Yewdall, S. J., Smith, J. M. A., Livingstone, J. C., Treffy, A., Luzzago, A., Levi, S., Arioso, P., Cesareni, G., Thomas, C. D., Shaw, W. V. & Harrison, P. M. (1991). *Nature (London)*, **349**, 541–544.

Magnus, K. A., Lattman, E. E., Volbeda, A. & Hol, W. G. J. (1991). *Proteins Struct. Funct. Genet.* **9**, 240–247.

Moore, G. R., Kadir, F. H. A., Al-Massad, F. K., Le Brun, N. E., Thomson, A. J., Greenwood, C., Keen, J. N. & Findlay, J. B. C. (1994). *Biochem. J.* **304**, 493–497.

Morris, A. L., MacArthur, M. W., Hutchinson, G. E. & Thornton, J. M. (1992). *Proteins Struct. Funct. Genet.* **12**, 345–364.

Navaza, J. (1992). *AMoRe: a New Package for Molecular Replacement.* In *Molecular Replacement*, edited by E. J. Dodson, S. Gover & W. Wolf, pp. 87–90. Warrington: Daresbury Laboratory.

Nordlund, P. & Eklund, H. (1993). *J. Mol. Biol.* **232**, 123–164.

Penfold, C. N., Ringeling, P. L., Moore, G. R., McEwan, A. G. & Spiro, S. (1996). *FEMS Microbiol. Lett.* **139**, 143–148.

Précigoux, G., Yariv, J., Gallois, B., Dautant, A., Courseille, C. & Langlois d'Estaintot, B. (1994). *Acta Cryst.* D**50**, 739–743.

Ramachandran, G. N. & Sasisekharan, V. (1968). *Adv. Protein Chem.* **23**, 283–337.

Rosenzweig, A. C., Frederick C. A., Lippard S. J. & Nordlund, P. (1993). *Nature (London)*, **366**, 537–542.

Rossmann, M. G. (1979). *J. Appl. Cryst.* **12**, 225–238.

Rossmann, M. G. & Blow, D. M. (1962). *Acta Cryst.* **15**, 24–31.

Rossmann, M. G., Leslie, A. G. W., Abdel-Meguid, S. S. & Tsukihara, T. (1979). *J. Appl. Cryst.* **12**, 570–581.

Roussel, A., Fontecilla-Camps, J. C. & Cambillau, C. (1990). *Acta Cryst.* A**46**, C66.

Sheriff, S. & Hendrickson, W. A. (1987). *Acta Cryst.* B**43**, 209–212.

Smith, J. M. A., Ford, G. C., Harrison, P. M., Yariv, J. & Kalb (Gilboa), A. J. (1989). *J. Mol. Biol.* **205**, 465–467.

St Pierre, T. G., Bell, S. H., Dickson, D. P. E., Mann, S., Webb, J., Moore, G. R. & Williams, R. J. P. (1986). *Biochim. Biophys. Acta*, **870**, 127–134.

Tong, L. & Rossmann, M. G. (1990). *Acta Cryst.* **A46**, 783–792.

Trikha, J., Theil, E. C. & Allewell, N. (1995). *J. Mol. Biol.* **248**, 949–967.

Yariv, J., Kalb (Gilboa), A. J., Sperling, R., Bauminger, E. R., Cohen, S. G. & Ofer, S. (1981). *Biochem. J.* **197**, 171–175.